

# CW Injection-locked Single Frequency Ti:Sapphire Laser

Li-Yueh Cheng  
National Tsing Hua University

July 26, 2004

Abstract

# CW Injection-locked Single Frequency Ti:Sapphire Laser

Li-Yueh Cheng

National Tsing Hua University

2004

A cw Ti:Sapphire laser wave injected with a single frequency diode laser is demonstrated. The injection-locked Ti:Sapphire laser has an advantage of a low threshold than conventional single-frequency Ti:Sapphire laser, because it eliminates the necessity of intracavity linewidth narrowing components. In comparison with MOPA, this method can provide higher intensity and better spatial mode quality.

Injection-locking a high power laser with a low power diode laser reproduces the diode laser at high power with good fidelity in frequency. The frequency shift and broadening of the Ti:Sapphire laser is measured using the method of beat note with the master laser. The linewidth is estimated as less than 5 MHz, and no shift is observed. The wavelength tuning range is determined by the tuning range of the laser diode used to inject the Ti:Sapphire laser.

Such a system can be a powerful tool for laser spectroscopy at a frequency region, where the high power single frequency diode laser is not available.

# Contents

<b>1</b>	<b>Introduction</b>	<b>1</b>
1.1	Injection-Locking Technique . . . . .	1
1.2	Ti:Sapphire Crystal . . . . .	1
<b>2</b>	<b>Fundamental Theory</b>	<b>3</b>
2.1	Injection-Locking Theory . . . . .	3
2.2	Motivation . . . . .	4
<b>3</b>	<b>Experiment</b>	<b>6</b>
3.1	Ti:Sapphire Laser . . . . .	6
3.2	Master Laser-Extended Cavity Diode Laser . . . . .	15
3.3	Frequency Modulation Spectroscopy . . . . .	16
3.3.1	The Electro-optic Effect of Anisotropic Media . . . . .	16
3.3.2	The Lithium Niobate Crystal . . . . .	17
3.3.3	The Pound-Drever-Hall Technique . . . . .	18
3.3.4	The Resonant Circuit . . . . .	23
3.4	Experimental Setup . . . . .	23
3.5	Frequency Shift and Linewidth Measurement . . . . .	24
<b>4</b>	<b>Results and Discussion</b>	<b>27</b>
4.1	Output Power of the Injection-locked Ti:Sapphire Laser . . . . .	27
4.2	Stability of the Injection-locked Ti:Sapphire Laser . . . . .	27
4.3	Frequency shift and Linewidth of the Injection-locked Ti:Sapphire Laser	30

5 Conclusion

35

# List of Figures

2.1	Schematic representation of the injection-locked laser model. . . . .	4
3.1	The water-cooled brass housing of the Ti:Sapphire crystal. . . . .	7
3.2	The Ti:Sapphire laser cavity. . . . .	8
3.3	The simulation for stability condition of the tangential part. . . . .	11
3.4	The simulation for stability condition of the sagittal part. . . . .	12
3.5	The calculated minimum difference of curvature between tangential part and sagittal part. . . . .	13
3.6	The calculated minimum difference of beam width between tangential part and sagittal part. . . . .	14
3.7	Expected error signal for $\omega_m = 10\Gamma$ , $M=0.1$ , line center $\Omega = 0$ . . . .	20
3.8	Expected error signal for $\omega_m = 0.01\Gamma$ , $M=0.1$ , line center $\Omega = 0$ . . .	21
3.9	Error signal when slave laser pumping is 1.2 W . . . . .	22
3.10	Error signal when slave laser pumping is 1.4 W . . . . .	22
3.11	The EOM resonant circuit . . . . .	23
3.12	A schematic diagram of the experiment layout, ECDL=extended cavity diode laser, PD=photodiode, PD2=fast photodiode, EOM=Electro-optic Modulator, MML=mode matching lens, PZT=piezoelectric transducer, HWP=half waveplate, LP=low pass filter . . . . .	25
3.13	The Fast Photodiode . . . . .	26
3.14	Feedback Loop . . . . .	26
4.1	pumping power vs. output power for the free-running Ti:Sapphire laser	28

---

4.2	pumping power vs. output power for the injection-locked Ti:Sapphire laser . . . . .	28
4.3	pumping power vs. output power for the Ti:Sapphire laser for injection-locked ( $\square$ ) and free-running ( $\triangle$ ) operation . . . . .	29
4.4	Power spectrum of the injection-locking Ti:Sapphire laser, while the slave laser pumping is 1.4 W . . . . .	30
4.5	Frequency beat note of the master laser and the Ti:Sapphire laser at 1.4 W pumping power. . . . .	32
4.6	Injection-locked Ti:Sapphire laser scanning Fabry-Perot signal at 1.4 W pumping power. The bottom curve shows the signal of the master laser. . . . .	33
4.7	Frequency beat note of the master laser and the Ti:Sapphire laser at 1.2 W pumping. . . . .	33
4.8	Frequency beat note of the master laser and the Ti:Sapphire laser at 1.4 W pumping. . . . .	34
4.9	Optical frequency spectrum of the laser. The top curve shows the spectrum of the injection-locked Ti:Sapphire laser at 1.4 W pumping power. The bottom curve shows the spectrum of the master laser. The curves are offset vertically for clarity. . . . .	34

# List of Tables

3.1	The Pockels Coefficients for $LiNbO_3$ . . . . .	17
-----	--------------------------------------------------	----

# Chapter 1

## Introduction

### 1.1 Injection-Locking Technique

Laser injection-locking was first demonstrated by Stover and Steier[1], who directly injected the beam of one He-Ne laser into the resonator of a second He-Ne laser. It has long been recognized as an effective technique for transferring the frequency stability of a low-power, well-stabilized master laser to a higher-power, less stable slave laser. Injection locking can also enforce unidirectional operation in ring laser system as well as single spatial or longitudinal mode operation. This technique has also been effectively used to improve the intensity noise of the injection-locked slave laser.

Injection locking has been used in a wide range of cw lasers, including Nd:YAG laser[2], He-Ne laser[3], VCSEL[4], argon-ion laser[5], erbium-doped fiber laser[6], and dye laser[7]. It has also been demonstrated for mode locked laser[8], Q-switch Ti:Sapphire laser[9].

### 1.2 Ti:Sapphire Crystal

Titanium-doped sapphire is one of the most commonly used crystals for wavelength tunable lasers today. The Titanium-sapphire laser was developed by Peter Moulton in the early 1980s and first reported by him in 1986. Ti:Sapphire lasers are solid-state

and optically pumped with a broad tunable range that makes them useful for many experiments. It offers a useful alternative to dye lasers, which wear out relatively quickly and often contain dangerous chemicals. A joint program between the NASA Langley Research Center and Union Carbide helped create Ti:Sapphire crystals of increasingly greater quality in the early 1990s, which NASA used to measure Tropospheric water vapor and aerosol profiles. The advent of diode-pumped Nd:YAG lasers in the 1990s also made them more useful and even easier to use by eliminating the need for temperamental argon-ion lasers as pump lasers.

The active ingredient of the laser medium is the  $Ti^{3+}$  ion, which substitutes the  $Al^{3+}$  ion in the sapphire ( $Al_2O_3$ ) host crystal. The sapphire host has excellent properties for laser medium including, high thermal conductivity, chemical inertness, and mechanical rigidity. The electron structure of the  $Ti^{3+}$  ion is a close shell plus a single 3d electron. The free-space, fivefold-degenerate (neglecting spin) d-electron levels are split by the crystal field of the host. The site for the  $Ti^{3+}$  ion has trigonal symmetry in the host  $Al_2O_3$ ; the crystal field can be viewed as sum of cubic- and trigonal-symmetry components. The cubic field dominates and splits the  $Ti^{3+}$  energy level into a triply degenerate  ${}^2T_2$  ground state and a doubly degenerate  ${}^2E$  excited state.

The absorption band of Ti:Sapphire is from about 450 to 600 nm, which makes it suitable for variety of laser pump sources - argon ion, frequency doubled Nd:YAG and YLF, copper vapour lasers. Titanium-doped sapphire generates continuous tunable radiation from about 680 to 1050 nm with peak power at 790 nm, and has relatively short fluorescence lifetime of 3.2  $\mu s$ . Because of 3.2  $\mu s$  fluorescence lifetime Ti:Sapphire crystals can be effectively pumped by short pulse flashlamps in powerful laser systems.

Titanium-doped sapphire has found many applications, characterized by a simple four level energy system, a broad tuning range, good efficiency, power handling, and a relative large gain cross-section. The Ti:Sapphire crystal demonstrates good operation in the pulse-periodic, quasi-cw, and cw modes of operation. Frequency doubling Ti:Sapphire laser can even provide tunable range over the blue-green region of the visible spectrum, and it is a leading material in the field of femtosecond pulse lasers.

# Chapter 2

## Fundamental Theory

### 2.1 Injection-Locking Theory

A general theory of injection-locking cw lasers is demonstrated in several publications. A brief method explains the injection locking phenomenon very well is based on Alder's model.[10]

In Alder's model, the eigenfield of the slave laser is given by:

$$E_S(t) = \varepsilon_S(t) \exp j [\omega_S t + \phi_S(t)] \quad (2.1)$$

Similarly, the eigenfield of the master laser has the same form:

$$E_M(t) = \varepsilon_M(t) \exp j [\omega_M t + \phi_M(t)] \quad (2.2)$$

$\varepsilon_S(t)$ ,  $\varepsilon_M(t)$  and  $\omega_S$ ,  $\omega_M$  represent the amplitude and angular frequency of the field of the slave and the master laser, respectively. Both the waves depend also on the phase  $\phi_{S,M}(t)$  which is given by:

$$\frac{d\phi_M(t)}{dt} + (\omega_M - \omega_S) = -\frac{\gamma_e \varepsilon_M(t)}{\varepsilon_S(t)} \sin [\phi_S(t) - \phi_M(t)] \quad (2.3)$$

where  $\gamma_e$  is the external decay rate.

Solving phase equation Eq. 2.3 under steady state condition gives the full locking

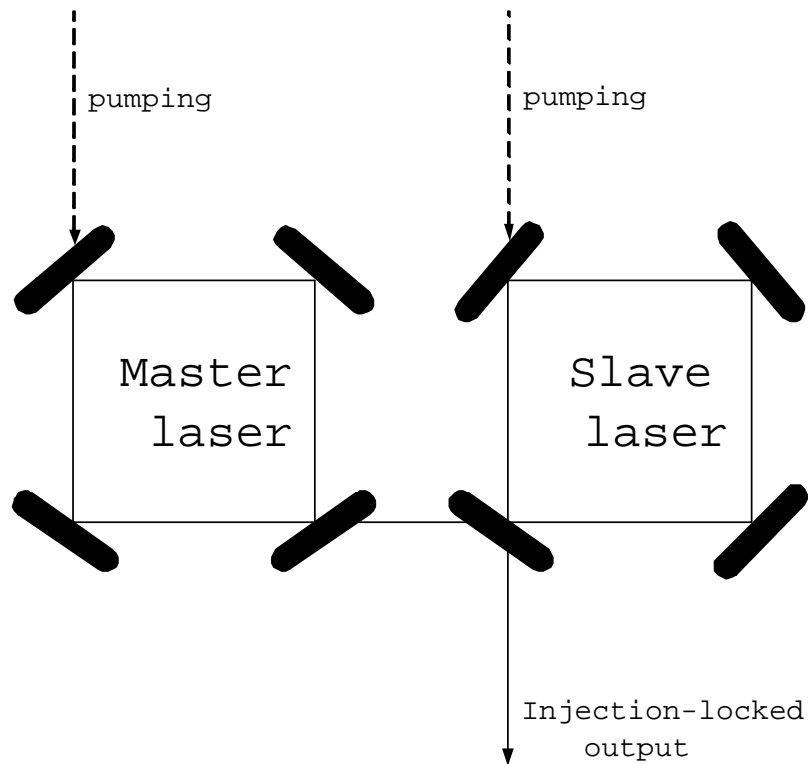


Figure 2.1: Schematic representation of the injection-locked laser model.

range, centered at resonance atomic transition frequency  $\omega_S$

$$\Delta\omega = \omega_M - \omega_S = 2\gamma_e \sqrt{\frac{I_M}{I_S}} \quad (2.4)$$

Fig. 2.1 shows the injection locking configuration. The master laser is injected into the slave laser. The master laser determines the output wavelength and forces both single-frequency and unidirectional operation. In other words, injection locking a high power slave laser with a low power single frequency master laser reproduce the master laser at higher power with good fidelity in frequency.

## 2.2 Motivation

1. Single-frequency and unidirectional operation without using optical diodes and birefringent filters.

2. Lower threshold power than conventional Ti:Sapphire lasers, therefore lower pumping power is requested. The typical threshold of a self-lasing cw single frequency Ti:Sapphire laser is 3-4 W. The 5 W or more green pumping source is a major investment of the entire Ti:Sapphire system. We are looking forward to a cw single frequency Ti:Sapphire laser with a threshold as low as 1 W, then the more popular, low-cost 3 W green frequency-doubled Nd:YAG can be used.
3. Reproducing the single-frequency, continuous-tunable, and lower-power master laser at relatively higher power.

# Chapter 3

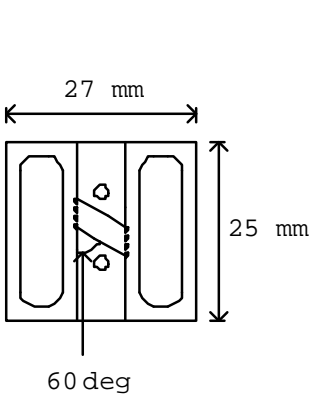
## Experiment

### 3.1 Ti:Sapphire Laser

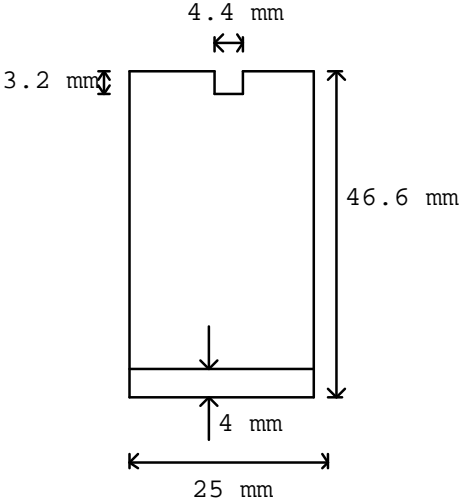
The Ti:sapphire crystal, used in our experiment is 10 mm long, 4 mm wide, and 3 mm high and mounted in a water-cooled brass housing, is typically sold with Brewster-cut faces. This means that the crystal faces are cut at an angle relative to the long axis of the crystal. With such faces polarized light incident on the crystal will experience no reflection loss, which is very desirable to optimize the intra-cavity losses.

Although Brewster-cut faces solve the problem of loss due to reflection, they create another problem—the astigmatism. Astigmatism is defined as a defect in an optical system in which light rays that originate at the same location fail to converge at a single focal point. More simply, astigmatism is when there is a different focus in two planes. Herwig W. Kogelnick discovered that introducing a folded cavity could compensate for this astigmatism. A folded cavity, which uses mirrors to reflect light in two dimensions rather than one, is more complicated than a straight one, but is a necessity if one wishes to minimize the effects of astigmatism and have a highly concentrated focal point.

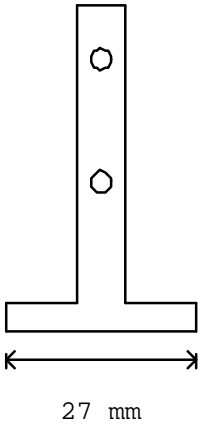
The Ti:Sapphire cavity, shown in Fig. 3.2, is a four-mirror folded cavity around a Ti:Sapphire crystal. All the four mirrors are made of BK7. The reflectivity of the flat output coupler ( $M4$ ) is 97%. The reflectivity of the other three mirrors, including two curved mirrors ( $M1, M2$ ) and one flat thin mirror ( $M3$ ), are all  $> 99.5\%$  at



Top view



Side view



Side view

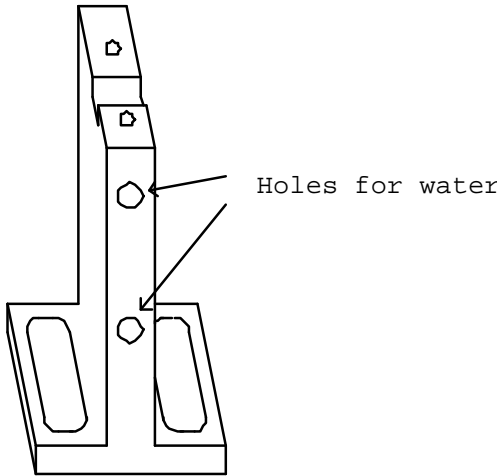


Figure 3.1: The water-cooled brass housing of the Ti:Sapphire crystal.

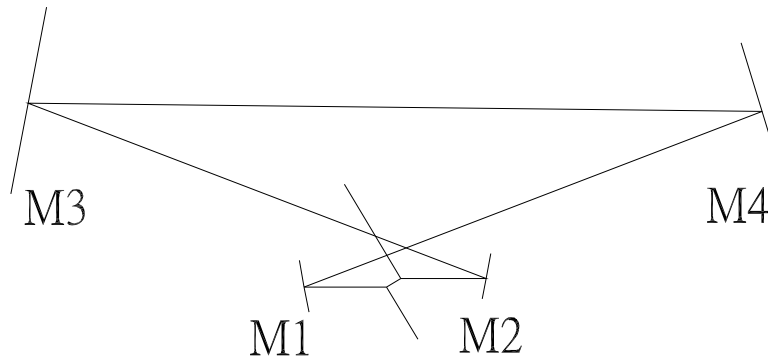


Figure 3.2: The Ti:Sapphire laser cavity.

650 nm-800 nm. These two curved mirrors are used to compensate the astigmatism introduced by the Brewster-cut crystal.

In order to obtain proper Rayleigh range, the distance between M1 and M4 (so as M2 and M3) is 300 mm, and the radius of curvature of M1 and M2 is 100 mm.

Ray matrices for paraxial elements are used to simulate our cavity. For the free-space region of refractive index  $n_0$  and length  $L$ , the ray matrix is:

$$\begin{bmatrix} 1 & \frac{L}{n_0} \\ 0 & 1 \end{bmatrix} \quad (3.1)$$

For the curved mirror, the ray matrix is:

$$\begin{bmatrix} 1 & 0 \\ \frac{-2}{R_e} & 1 \end{bmatrix} \quad (3.2)$$

where  $R_e = R \cos \theta$  for the incident light is in the plane of incidence (tangential), and  $R_e = \frac{R}{\cos \theta}$  for the incident light is perpendicular to the plane of incidence (sagittal). (R:radius;  $\theta$ :incident angle)

For the flat mirror, the ray matrix is:

$$\begin{bmatrix} 1 & 0 \\ 0 & 1 \end{bmatrix} \quad (3.3)$$

When the light transmit from free space into the Ti:Sapphire crystal, the ray matrix for the tangential part is:

$$\begin{bmatrix} \frac{\cos \theta_t}{\cos \theta_i} & 0 \\ 0 & \frac{\cos \theta_i}{\cos \theta_t} \end{bmatrix} \quad (3.4)$$

$\theta_i$  is the angle of incidence, and  $\theta_t$  is the angle of refraction. Because of the Brewster cut of the Ti:Sapphire crystal,  $\theta_i$  and  $\theta_t$  satisfy the equation:

$$\begin{aligned} \theta_i + \theta_t &= 90^\circ \\ \frac{\cos \theta_t}{\cos \theta_i} &= \frac{\sin \theta_i}{\sin \theta_t} = \frac{n_{ti-sa}}{n_{free-space}} = \frac{n_{ti-sa}}{1} \equiv n \end{aligned} \quad (3.5)$$

Eq. 3.4 can be written as:

$$\begin{bmatrix} n & 0 \\ 0 & \frac{1}{n} \end{bmatrix} \quad (3.6)$$

When the light transmit from free space into the Ti:Sapphire crystal, the ray matrix for the sagittal part is simply a  $2 \times 2$  unit matrix.

Let the ray matrix for propagation through one period of our cavity, from an arbitrary reference plane in one period to the corresponding plane one period later, be denoted by  $\mathbf{M}$ .

$$\mathbf{M} = \begin{bmatrix} A & B \\ C & D \end{bmatrix} \quad (3.7)$$

Considering the stability condition:

$$\left( \frac{A + D}{2} \right)^2 \leq 1 \quad (3.8)$$

The simulation for tangential and sagittal part is shown in Fig. 3.3 and Fig. 3.4, respectively. One of the axes is the distance between M1 (M2) and the Ti:Sapphire

crystal. The other is two times of the incident angle on curved mirrors. The distance between M1 (M2) and the Ti:Sapphire crystal is then determined to be 50.8 mm.

The wavefront radius of curvature is:

$$R = \frac{2B}{D - A} \quad (3.9)$$

The calculated difference of curvature between tangential part and sagittal part is shown in Fig. 3.5

The beam width is:

$$W = \frac{\lambda}{\pi} \sqrt{\left| \frac{2B}{\sqrt{4 - (A + D)^2}} \right|} \quad (3.10)$$

The calculated difference of beam width between tangential part and sagittal part is shown in Fig. 3.6

Under considering the minimum difference of radius of curvature and beam width, the incident angle at curved mirrors is  $10.5^\circ$ .

### Finesse and Spectral Width of the Ti:Sapphire Cavity

The effective overall distributed-loss coefficient  $\alpha_r$  is:

$$\alpha_r = \alpha_s + \frac{1}{2d} \times \ln \frac{1}{R_1 R_2 R_3 R_4} \quad (3.11)$$

where  $\alpha_s$  is the loss coefficient of the laser medium, and  $d \sim 1160$  mm is the optical length of the Ti:Sapphire cavity. We assume that  $\alpha_s \approx 0$ ,  $R_1 = R_2 = R_3 \approx 99.5\%$ , and  $R_4 \approx 97\%$ . Eq. 3.11 can be written as:

$$\begin{aligned} \alpha_r &\approx \frac{1 - R_1}{2d} + \frac{1 - R_2}{2d} + \frac{1 - R_3}{2d} + \frac{1 - R_4}{2d} \\ &= \frac{0.045}{2d} \end{aligned} \quad (3.12)$$

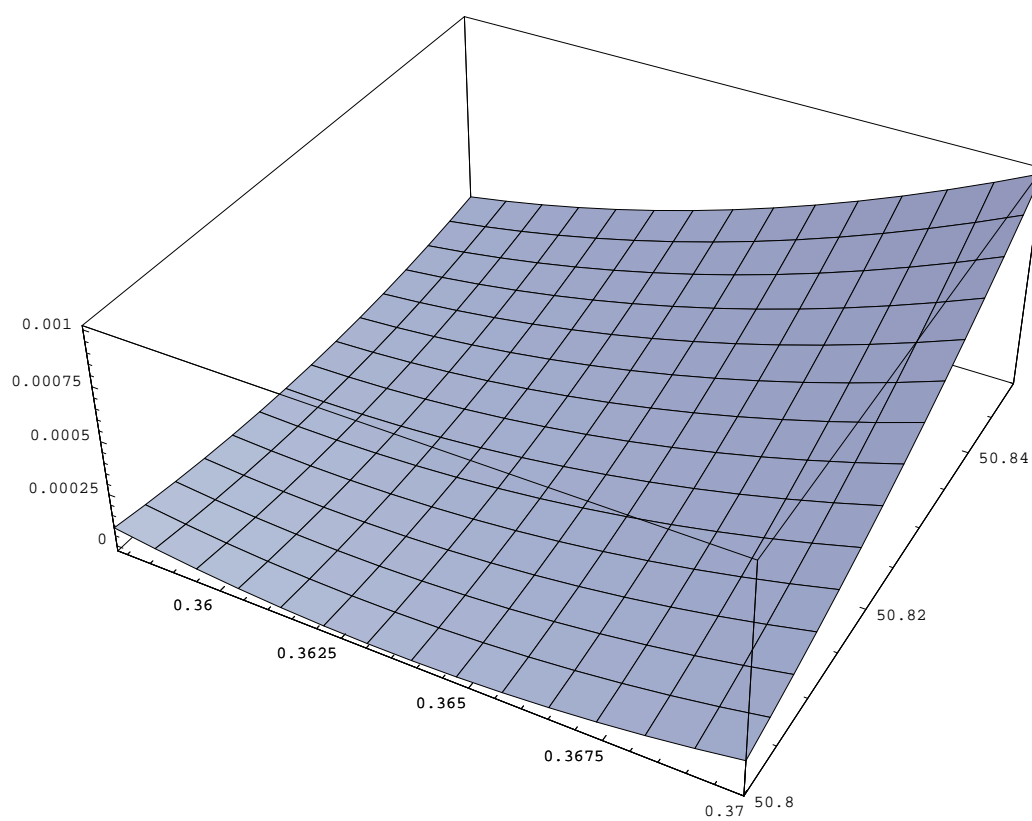


Figure 3.3: The simulation for stability condition of the tangential part.

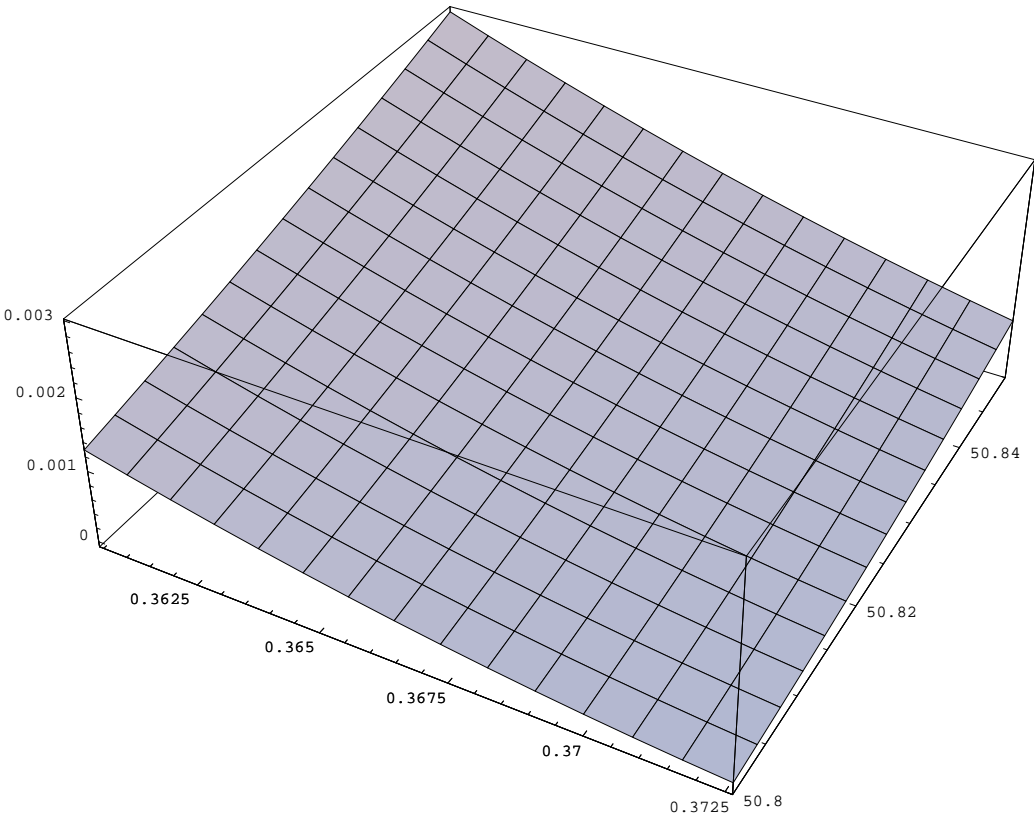


Figure 3.4: The simulation for stability condition of the sagittal part.

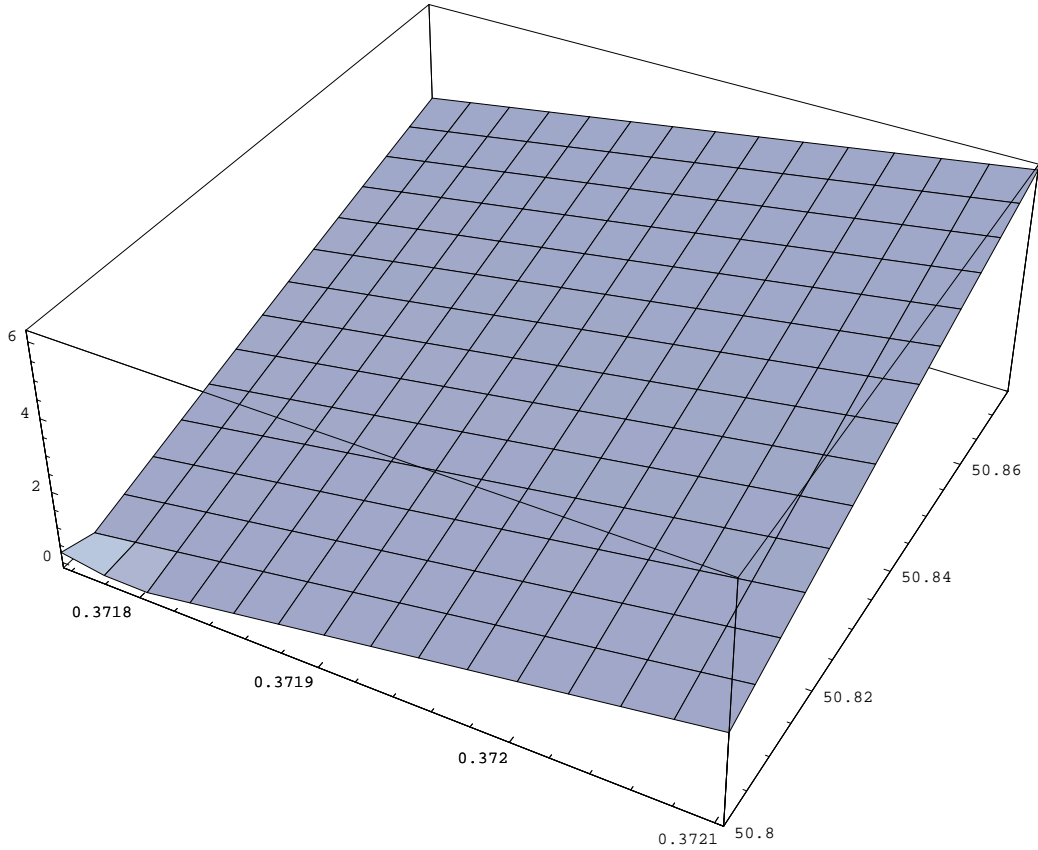


Figure 3.5: The calculated minimum difference of curvature between tangential part and sagittal part.

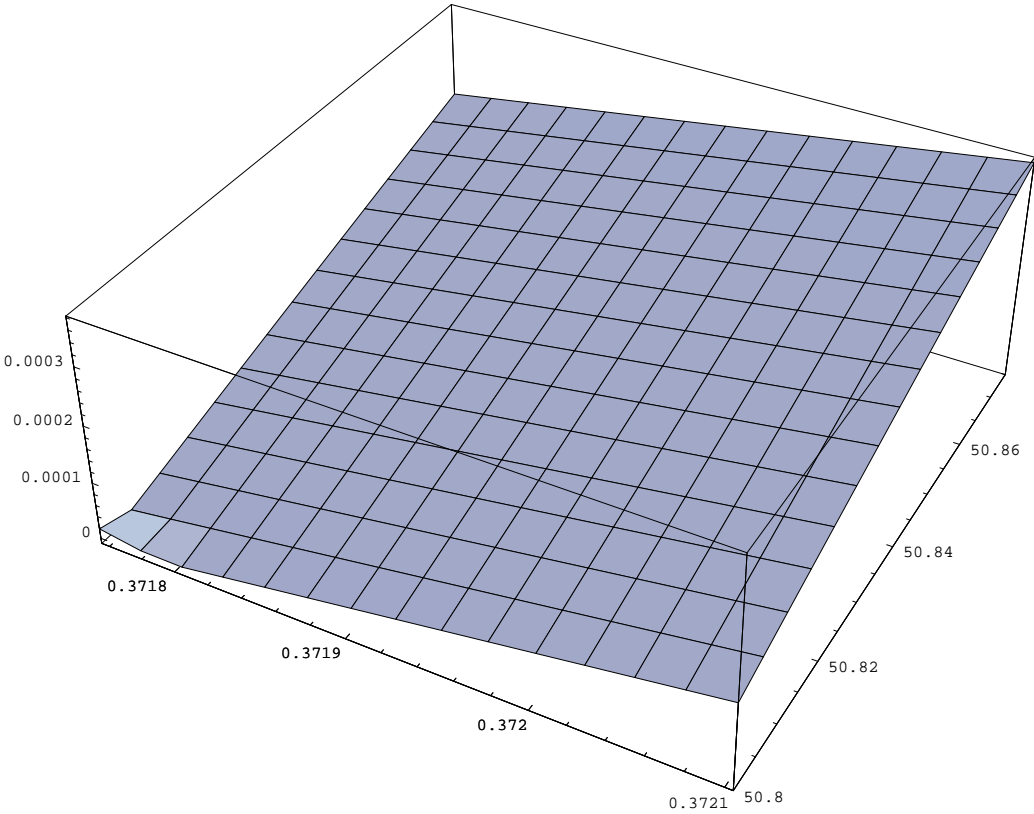


Figure 3.6: The calculated minimum difference of beam width between tangential part and sagittal part.

Because  $\alpha_r d \ll 1$ , the **finesse** of the resonator is:

$$\begin{aligned}
 F &\approx \frac{\pi}{\alpha_r d} \\
 &\approx \frac{2\pi}{0.045} \\
 &= 139.6 \gg 1
 \end{aligned} \tag{3.13}$$

Free spectrum range of our cavity is:

$$\begin{aligned}
 \text{F.S.R} &= \frac{c}{d} \\
 &= \frac{3 \times 10^{11}}{1160} \\
 &= 258.6 \text{MHz}
 \end{aligned} \tag{3.14}$$

Because  $F \gg 1$ , the width of the resonances  $\delta\nu$ :

$$\begin{aligned}
 \delta\nu &\approx \frac{\nu_F}{F} \\
 &> \frac{258.6 \text{MHz}}{139.6} \\
 &\approx 1.85 \text{MHz}
 \end{aligned} \tag{3.15}$$

## 3.2 Master Laser-Extended Cavity Diode Laser

The master laser is the Sanyo DL7140-201S within an extended cavity configuration (ECDL) at 785 nm. The light emitted from the front facet of the laser diode is collimated by a multi-element lens with a very short focal length (diffraction-limit) and then hits a reflective grating. The grating is adjusted in the so-called Littrow configuration. In the Littrow configuration, the grating is aligned so that the first order diffracted beam goes back directly into the laser. The coarse lasing wavelength is determined by the angle of the grating with respect to the laser, wavelength tuning is accomplished by changing this angle. The zero order reflected beam is the output. This configuration offers the advantage that almost the entire laser output is available for the experiment. A disadvantage is that the angle of the output beam changes slightly as the laser is tuned with the diffraction grating angle.

### 3.3 Frequency Modulation Spectroscopy

#### 3.3.1 The Electro-optic Effect of Anisotropic Media

The optical properties of anisotropy crystals are described by the index ellipsoid: [12]

$$\frac{x^2}{(n_x)^2} + \frac{y^2}{(n_y)^2} + \frac{z^2}{(n_z)^2} = 1 \quad (3.16)$$

where the x,y and z are chosen to be in the same direction as the principal axes of a crystal. For a uniaxial crystal, the index ellipsoid takes the simple form:

$$\frac{x^2}{n_o^2} + \frac{y^2}{n_o^2} + \frac{z^2}{n_e^2} = 1 \quad (3.17)$$

where the optic axis (axis of symmetry) is in the z-direction. By convention,  $n_o$  and  $n_e$  are the ordinary and extraordinary refractive indices respectively.

The *electro-optic effect* is the change in the refractive index resulting from the application of a electric field. The magnitude and direction of the induced change in the refractive index depend on the magnitude and direction of the applied field relative to the dielectric axes of the crystal.

The refractive index changes in proportion to the applied electric field, in which case the effect is known as the linear electro-optic effect or the Pockels effect. The effect of the electric field may be described by a modified index ellipsoid:

$$\sum_{ij} \eta_{ij}(E) x_i x_j = 1 \quad (3.18)$$

where  $\eta_{ij}(E)$  is the impermeability tensor, determined by

$$\eta_{ij}(E) = \eta_{ij}(0) + \sum_k \gamma_{ijk} E_k \quad (3.19)$$

where  $\eta_{ij}(0)$  is a diagonal matrix with elements  $\frac{1}{(n_1)^2}$ ,  $\frac{1}{(n_2)^2}$ , and  $\frac{1}{(n_3)^2}$ , and  $\gamma_{ijk}$  is the Pockels Coefficients.[12]

### 3.3.2 The Lithium Niobate Crystal

Lithium Niobate is a trigonal 3m crystal, negative uniaxial crystal. The Pockels Coefficients are listed in table 3.3.2.[13]

Pockels Coefficients $10^{-12}m/V$	Refractive Index
$\gamma_{33}=30.8$	$n_o=2.29$
$\gamma_{13}=8.6$	
$\gamma_{22}=3.4$	$n_e=2.20$
$\gamma_{42}=28$	

Table 3.1: The Pockels Coefficients for  $LiNbO_3$

The Electro-optic Tensor is:

$$\begin{bmatrix} 0 & -\gamma_{22} & \gamma_{13} \\ 0 & \gamma_{22} & \gamma_{13} \\ 0 & 0 & \gamma_{33} \\ 0 & \gamma_{42} & 0 \\ \gamma_{42} & 0 & 0 \\ -\gamma_{22} & 0 & 0 \end{bmatrix} \quad (3.20)$$

The crystal used in this experiment is 15 mm long, 3 mm wide and 3 mm high. It is clamped between two electrodes so that a transverse electric field could be applied along the optic axis (z-direction). Under such condition the crystal remains uniaxial, but with a modified index ellipsoid:

$$\left[ \frac{1}{n_o^2} + \gamma_{13}E \right] (x^2 + y^2) + \left[ \frac{1}{n_e^2} + \gamma_{33}E \right] z^2 = 1 \quad (3.21)$$

Light propagates through the crystal with the axis of polarization parallel to the

optic axis. Light therefore experiences a variable refractive index given by[12]

$$n_e(E) = n_e - \frac{1}{2}n_e^3\gamma_{33}E \quad (3.22)$$

Consequently the application of an electric field changes the output phase of light passing through the crystal by an amount:

$$\delta = \frac{\pi L}{\lambda_0 d}n_e^3\gamma_{33}V \quad (3.23)$$

where  $V$  is the applied voltage,  $L$  is the crystal length,  $d$  is the width of the crystal along the direction of applied electric field and  $\lambda_0$  is the free-space wavelength of light.

For the crystal used in our experiment, Eq. 3.23 gives an expected phase per unit of applied voltage of:

$$\delta/V = 6.62 \times 10^{-3}rad/V \quad (3.24)$$

### 3.3.3 The Pound-Drever-Hall Technique

The first step of locking procedure is to generate an error signal for locking the Ti:Sapphire cavity to the master laser. The two most convenient methods for generating an error signal are side-locking and the Pound-Drever-Hall technique. The side-locking method has been used in our experiment, in order to lock the external cavity diode laser to a reference cavity for frequency stability of the diode laser. In order to lock the Ti:Sapphire cavity to the diode laser, we have to use the Pound-Drever-Hall technique rather than side-locking technique. Because the slightly off-resonance between the Ti:Sapphire laser and the master laser, buildup of optical power in the cavity will be reduced, and noise on the transmitted intensity increases.

The Pound-Drever-Hall technique circumvents the drawback by modulating the light at high frequency, where the technical noise is near the shot-noise limit. The resulting error signal has a high signal-to-noise ratio, which can provide a robust lock. Furthermore, the error signal has odd symmetry about the line center that enables locking to the center of a cavity fringe. For these reasons, we prefer the Pound-Drever-

Hall technique for locking the Ti:Sapphire cavity to the diode laser.

Frequency modulation of the light transmitted by the lithium niobate crystal can be achieved by the application of a sinusoidal varying electric field. The effect of an applied voltage of the form  $V = V_0 \sin \omega_m t$  is to change the output phase of the light by:

$$M \sin \omega_m t = \frac{\pi L}{\lambda_0 d} n_e^3 \gamma_{33} V_0 \sin \omega_m t \quad (3.25)$$

If the electric field of the incident light is described by  $E_{in}(t) = E_0 \exp(i\omega_0 t)$ , then the field of the transmitted light can be written as: [14]

$$\begin{aligned} E_{out}(t) &= E_0 \exp[i(\omega_0 t + M \sin \omega_m t)] \\ &= E_0 \exp[i\omega_0 t] \sum_{n=-\infty \rightarrow \infty} J_n(M) \exp(in\omega_m t) \\ &= E_0 \exp[i\omega_0 t] \left[ J_0(M) + J_1(M) \exp(i\omega_m t) + J_{-1}(M) \exp(-i\omega_m t) \right. \\ &\quad \left. + J_2(M) \exp(i2\omega_m t) + J_{-2}(M) \exp(-i2\omega_m t) + \dots \right] \end{aligned} \quad (3.26)$$

Frequency sideband, separated by the modulation frequency  $\omega_m$ , are therefore generated. Because  $J_{-n}(M) = (-1)^n J_n(M)$ , the lower-frequency component with odd  $n$  are  $180^\circ$  out of phase from the upper sidebands, as required for FM spectroscopy.

The optical field defined by Eq. 3.26 is passed through a sample (the cavity) that contains an absorption line of spectrum width  $\Gamma$ . The effect of the sample for each frequency component  $\omega_n$  can be written as the transmission function  $T(\omega_n) = \exp(-\delta_n - i\phi_n)$ , where  $\delta_n$  is the field amplitude attenuation and  $\phi_n$  is the optical phase shift at  $\omega_n$ . The transmitted field is than [14]

$$E_T(t) = E_0 \exp[i\omega_0 t] \sum_{n=-\infty \rightarrow \infty} T(\omega_n) J_n(M) \exp(in\omega_m t) \quad (3.27)$$

The typical FM spectroscopy situation involves only one pair of sidebands. Because  $M$  is typically small than 1,  $J_n(M)$  is negligible for  $n > 1$ . Eq. 3.27 can be

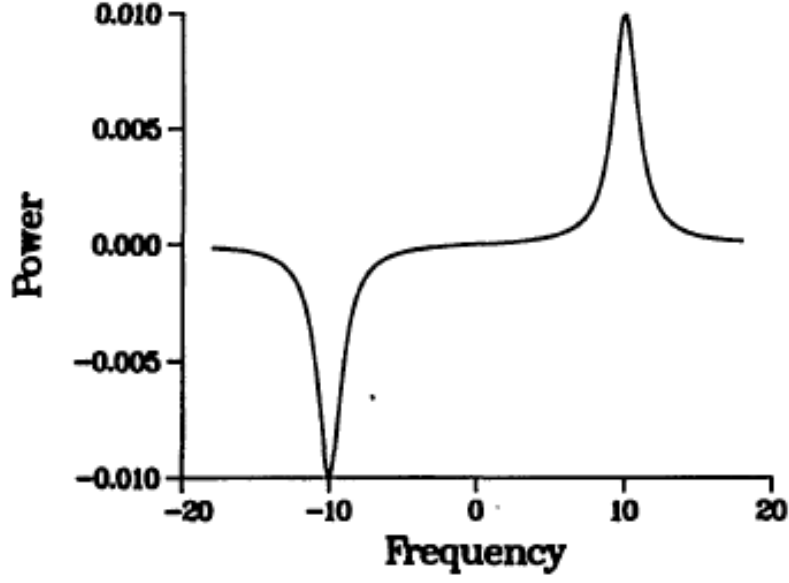


Figure 3.7: Expected error signal for  $\omega_m = 10\Gamma$ ,  $M=0.1$ , line center  $\Omega = 0$

simplified as:

$$|E^2(t)| = E_0^2 \exp(-2\delta_0) [1 + M(\delta_{-1} - \delta_1) \cos \omega_m t + M(\phi_{-1} + \phi_1 - 2\phi_0) \sin \omega_m t] \quad (3.28)$$

The  $\sin \omega_m t$  component represents three dispersion curves. When  $\omega_m \gg \Gamma$ , the  $\cos \omega_m t$  term displays the line shape of the absorption profile. The Lorentzian absorption profile is assumed:

$$\delta(\omega) = \frac{A\Gamma^2}{(\omega - \Omega)^2 + \Gamma^2} \quad (3.29)$$

$\Omega$  is the central frequency and  $A$  is the amplitude of absorption profile.

The cosine term of Eq. 3.28 is

$$\begin{aligned} I &= \exp(-2\delta_0) M (\delta_{-1} - \delta_1) \\ &= \exp(-2\delta_0) M \left[ \frac{A\Gamma^2}{(\omega - \omega_m - \Omega)^2 + \Gamma^2} - \frac{A\Gamma^2}{(\omega + \omega_m - \Omega)^2 + \Gamma^2} \right] \end{aligned} \quad (3.30)$$

For the case of  $M \ll 1$  and  $\omega_m \gg \Gamma$ , we can expect the error signal, shown in Fig. 3.7.[14]

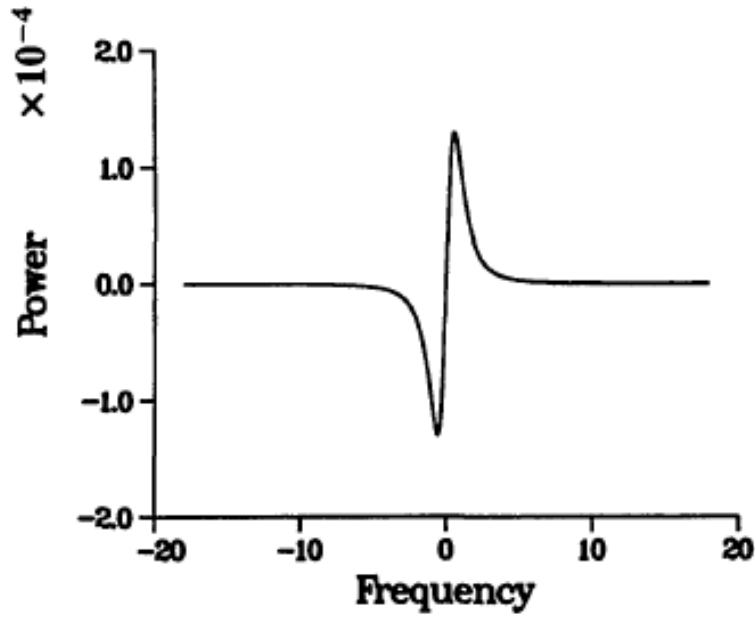


Figure 3.8: Expected error signal for  $\omega_m = 0.01\Gamma$ ,  $M=0.1$ , line center  $\Omega = 0$

Furthermore, decreasing  $\omega_m$  decreases the peak spacing, the expected error signal is in Fig. 3.8. The error signal of the Ti:Sapphire laser cavity with 1.2 W pumping (below the threshold power 1.23 W) and 1.4 W pumping power are shown in Fig. 3.9 and Fig. 3.10, respectively. Note that certain optical feedback affects the master laser and then decreases the signal-to noise ratio of the locking error signal, when the pumping power is above the threshold. Note that the width of the cavity without pumping is 1.85 MHz, and the modulation frequency  $\omega_m$  is 5.82 MHz.

The ratio of the amplitude of the first sideband to that of the carrier is given by:

$$\frac{E_1}{E_0} = \frac{J_1(M)}{J_0(M)} \quad (3.31)$$

Typically, the ratio used in the FM spectroscopy is  $\sim 15\%$ . Solving Eq. 3.28 graphically shows that this corresponds to a modulation index of  $M = 0.75$ . It shows that the amplitude of the sinusoidal voltage applied to the crystal must be  $\sim 113.56$  V from Eq. 3.23.

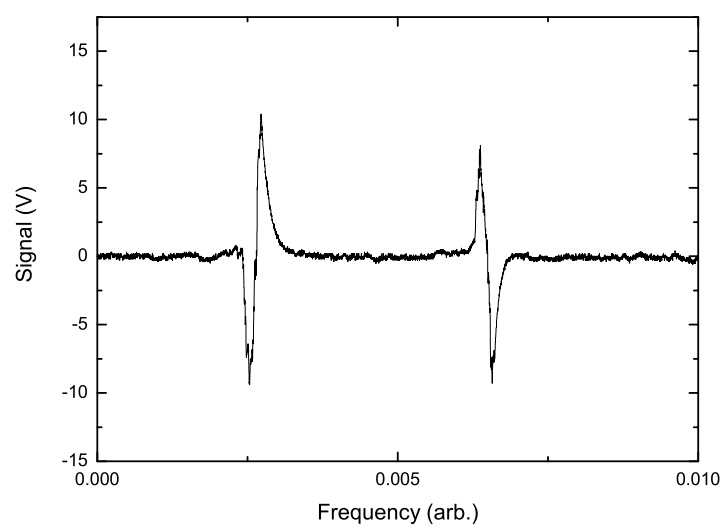


Figure 3.9: Error signal when slave laser pumping is 1.2 W

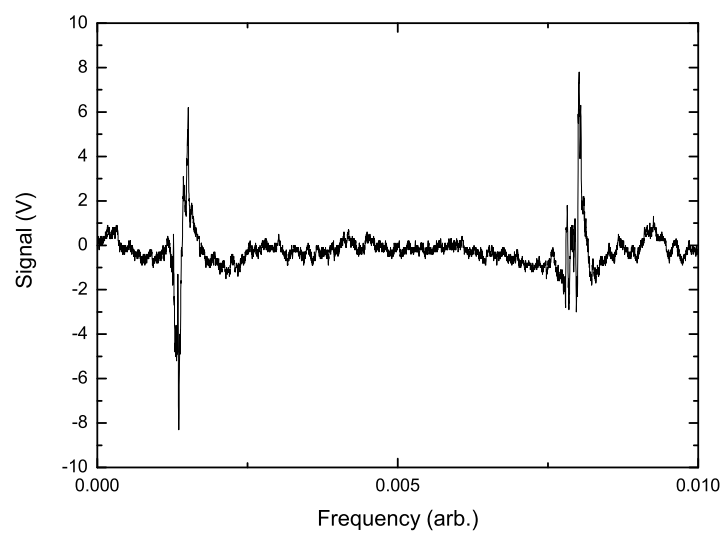


Figure 3.10: Error signal when slave laser pumping is 1.4 W

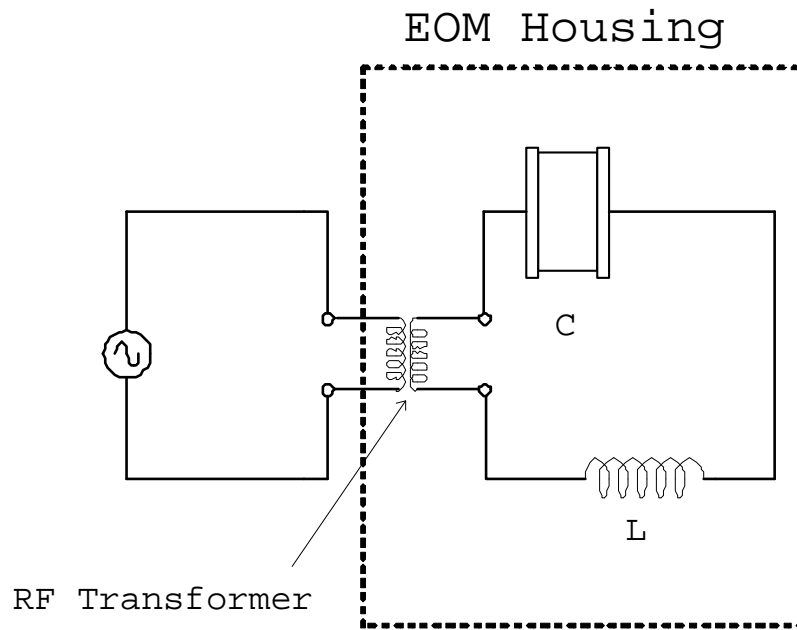


Figure 3.11: The EOM resonant circuit

### 3.3.4 The Resonant Circuit

The method of achieving the required high modulation voltage at a radio frequency (RF) desirable in FM spectroscopy is to incorporate the electro-optic crystal into a resonant circuit of high Q factor. The circuit, with the resonant frequency  $\omega = \frac{1}{\sqrt{LC}} \equiv \omega_m$ , used in our experiment is illustrated in Fig. 3.11. The RF transformer amplifies the RF signal twice as much. **L** represents an inductor with high Q-factor, and **C** means the capacitance of the gold electrode coated lithium niobate crystal. The output of a RF function generator (Hewlett Packard 33120A) is amplified (Mini-Circuits RF Amplifier ZHL-3A) and applied to the resonant circuit via a BNC connection on the outside of the EOM housing.

The final circuit arrangement for the EOM use a inductor of  $L = 4.7\mu H$ . This produces a resonant frequency of  $\sim 5.82$  MHz.

## 3.4 Experimental Setup

Experimental setup for our system is shown in Fig. 3.12.

Two isolators prevent optical feedback and rotate the polarization of the master laser from s to p. The master laser is preliminary stabilized on a tunable 500 MHz F.S.R (free spectrum range) reference cavity, made of Invar, by the side-locking method. The linewidth of the diode laser is about 1 MHz. The focal length of the mode matching lens in the diode laser beam is 750 mm.

Up to 2 W from the 532 nm pump laser is focused into the middle of the Ti:Sapphire crystal. The half waveplate in the green beam is a wave retarder represented by this matrix:

$$\begin{bmatrix} 1 & 0 \\ 0 & \exp(-j\pi) \end{bmatrix} \quad (3.32)$$

The retarder converts linearly polarized light  $\begin{bmatrix} \cos\theta \\ \sin\theta \end{bmatrix}$  into linear polarized light  $\begin{bmatrix} \cos\theta \\ -\sin\theta \end{bmatrix}$ , thus rotating the plane of polarization by  $2\theta$ . Note that  $\theta$  is the angle between the fast axis of the retarder and the polarization direction of the light. In other words, we can rotate the plane of polarization by any angle by rotating the axes of the retarder for the light of certain polarization. The half waveplate in our experiment thus rotates the plane of polarization of a linearly polarized green beam into p-polarization. With such polarization, light incident on the Brewster-cut Ti:Sapphire crystal will experience no reflection loss.

The scanning Fabry Perot is used to diagnose the laser mode.

Fast-photodiode: Fig. 3.13.

Servo loop: Fig. 3.14.

Mixer: Mini-Circuits ZAD-1.

### 3.5 Frequency Shift and Linewidth Measurement

After the injection-locked Ti:Sapphire output beam passing through an AOM (Acousto-Optic Modulator), we select the +1st order diffracted beam Fig. 3.12. Its frequency has been shifted by +80 MHz. The beat note, monitor by a spectrum analyzer, is use to determine the linewidth of the injection-locked Ti:Sapphire laser and the frequency shift between the injection-locked Ti:Sapphire laser and the master laser.

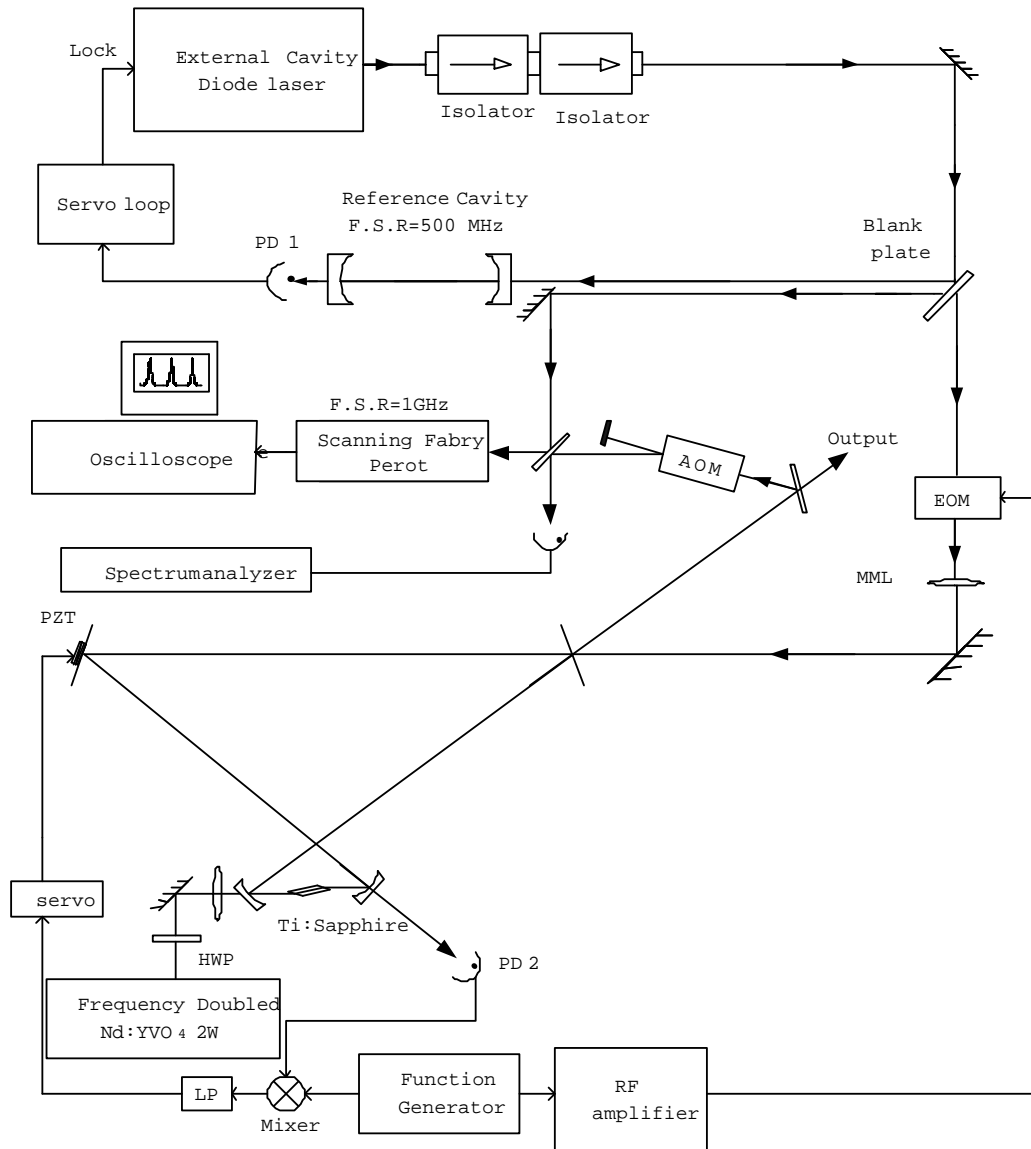


Figure 3.12: A schematic diagram of the experiment layout, ECDL=extended cavity diode laser, PD=photodiode, PD2=fast photodiode, EOM=Electro-optic Modulator, MML=mode matching lens, PZT=piezoelectric transducer, HWP=half waveplate, LP=low pass filter

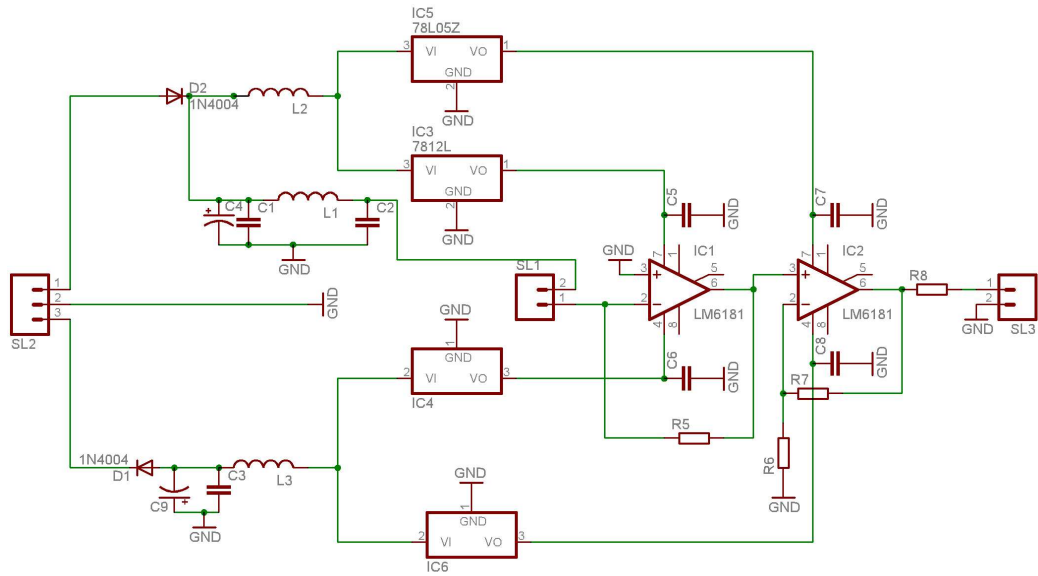


Figure 3.13: The Fast Photodiode

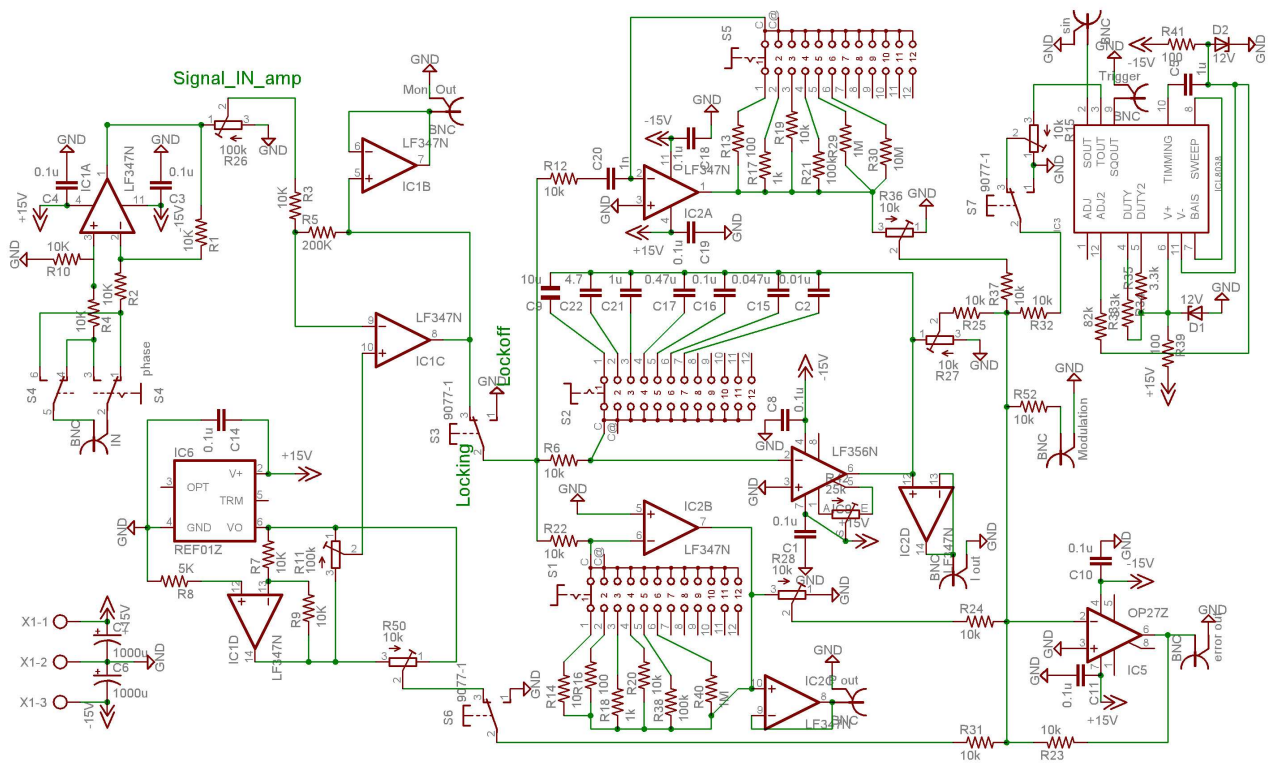


Figure 3.14: Feedback Loop

# Chapter 4

## Results and Discussion

### 4.1 Output Power of the Injection-locked Ti:Sapphire Laser

Fig. 4.1 shows the pumping power versus output power of the free-running Ti:Sapphire laser. Without injection locking, the laser does not oscillate until photons are spontaneously emitted into the cavity mode. The threshold is 1.23 W. Our measured slope efficiency is about 23%. Fig. 4.2 shows a plot of the power out of the injection-locked Ti:Sapphire laser. Because the master laser puts photons into the cavity, the injection-locked Ti:Sapphire laser can oscillate at pump powers below the non-injected threshold. Note that certain optical feedback affects the master laser and then decreases the signal-to-noise ratio of the locking error signal. Because of optical feedback, injection-locking operation under the condition of pumping power above 2 W cannot be achieved, while the locking error signal becomes too noisy.

### 4.2 Stability of the Injection-locked Ti:Sapphire Laser

The power spectrum of the injection-locked Ti:Sapphire laser from 0 to 250 kHz is shown in Fig. 4.4. It falls rapidly in 1 kHz, more slowly to 50 kHz, and is flat at higher

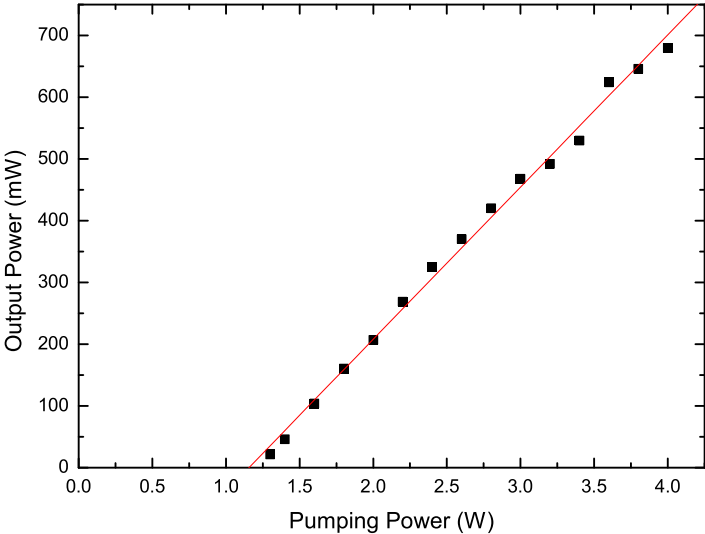


Figure 4.1: pumping power vs. output power for the free-running Ti:Sapphire laser

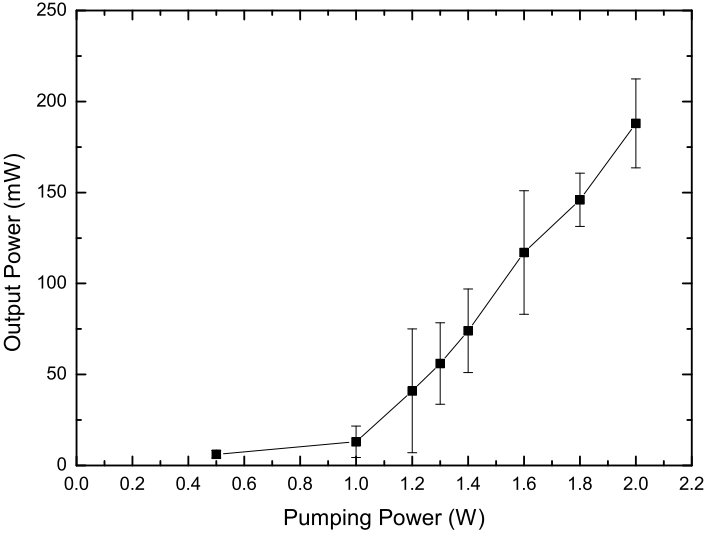


Figure 4.2: pumping power vs. output power for the injection-locked Ti:Sapphire laser

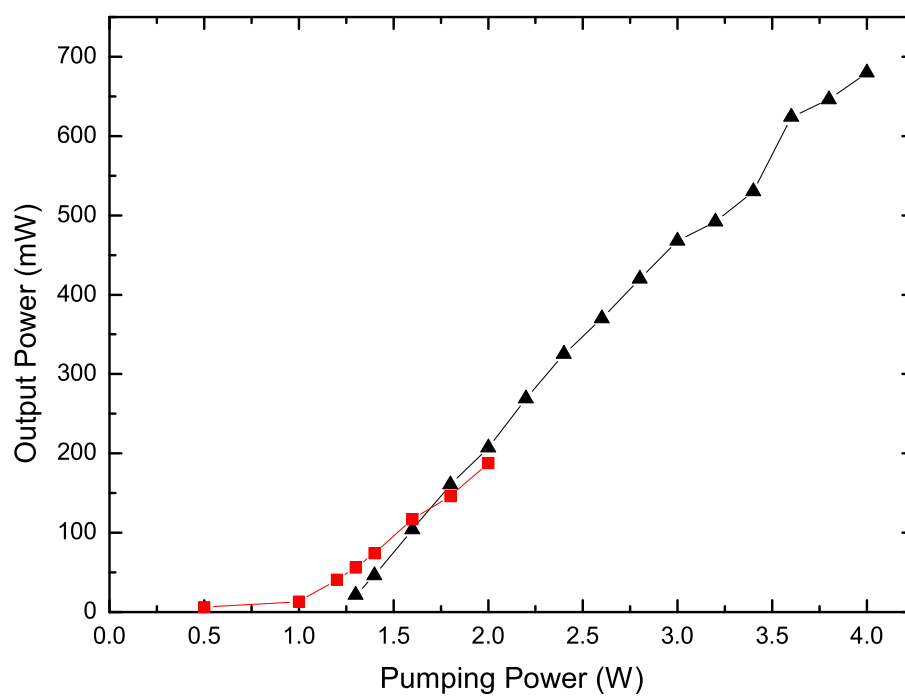


Figure 4.3: pumping power vs. output power for the Ti:Sapphire laser for injection-locked (□) and free-running (△) operation

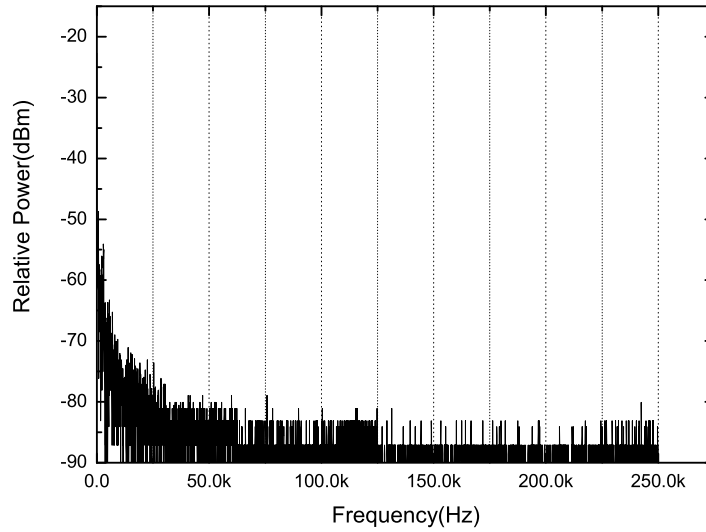


Figure 4.4: Power spectrum of the injection-locking Ti:Sapphire laser, while the slave laser pumping is 1.4 W

frequency. We conclude that the noise is mainly from the vibration and acoustic noise. A more rigid, stable Ti:Sapphire laser cavity could improve the power stability.

### 4.3 Frequency shift and Linewidth of the Injection-locked Ti:Sapphire Laser

Fig. 4.5 shows the injection locking condition. As the injected signal wavelength is inside the locking range, the slave laser action is destroyed due to gain quenching by the injected laser, as shown in Fig. 4.5(a). [6] After successful injection locking, a single-mode operation of the laser is verified, as shown in Fig. 4.5(b).

Fig. 4.6 shows the injection-locked Ti:Sapphire laser scanning Fabry-Perot signal at 1.4 W pumping power with output power of 80 mW. The single mode master laser reproduces at higher power with good fidelity.

Fig. 4.7 and Fig. 4.8 are the spectrum analyzer signals of 1.2 W and 1.4 W pumping power, respectively. The central frequency of the beat note is about 80 MHz, due to

the shift of the master laser in AOM. The frequency position indicates that the slave laser has the same frequency as the master laser and the narrow linewidth shows that they are highly correlated under injection-locking.

The measurement mentioned in **section 3.5** cause a problem that the spectrum analyzer signal contains also the beat note of the diode laser and the diode laser itself reflected from the flat output coupler of the Ti:Sapphire cavity. Therefore the measurement of the linewidth of the injection-locked Ti:Sapphire laser can not be extracted from Fig. 4.7 and Fig. 4.8. However, we can estimate roughly that less than 5 MHz linewidth is obtained.

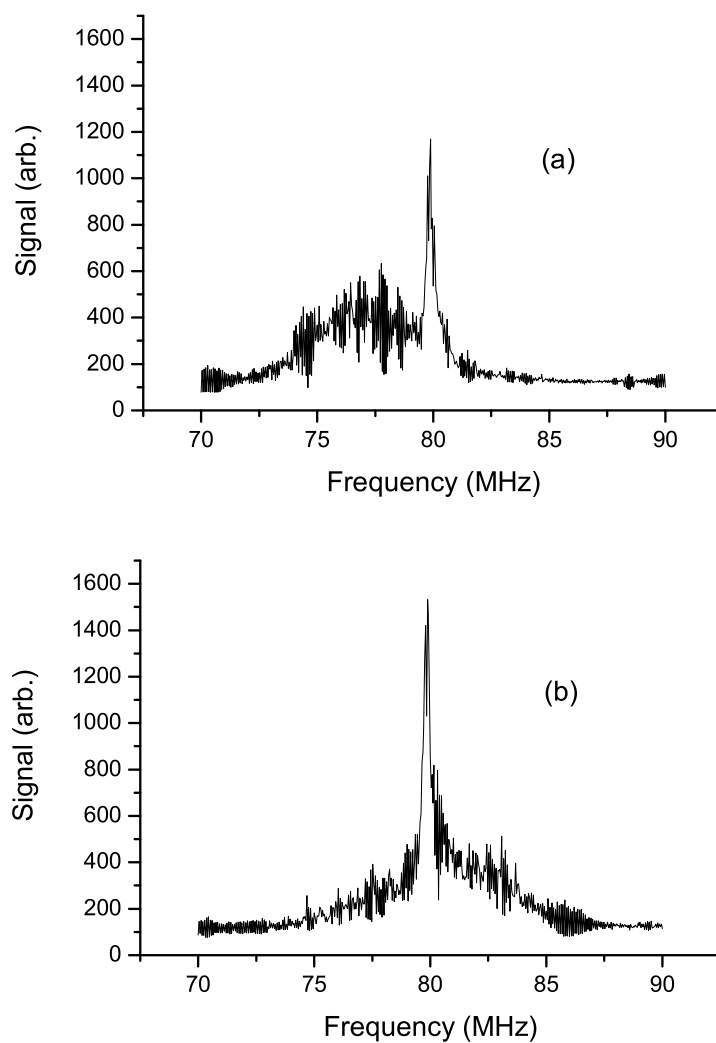


Figure 4.5: Frequency beat note of the master laser and the Ti:Sapphire laser at 1.4 W pumping power.

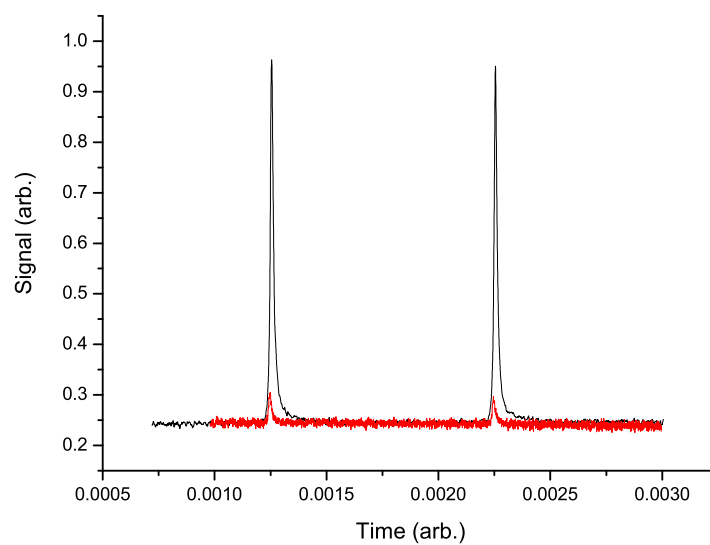


Figure 4.6: Injection-locked Ti:Sapphire laser scanning Fabry-Perot signal at 1.4 W pumping power. The bottom curve shows the signal of the master laser.

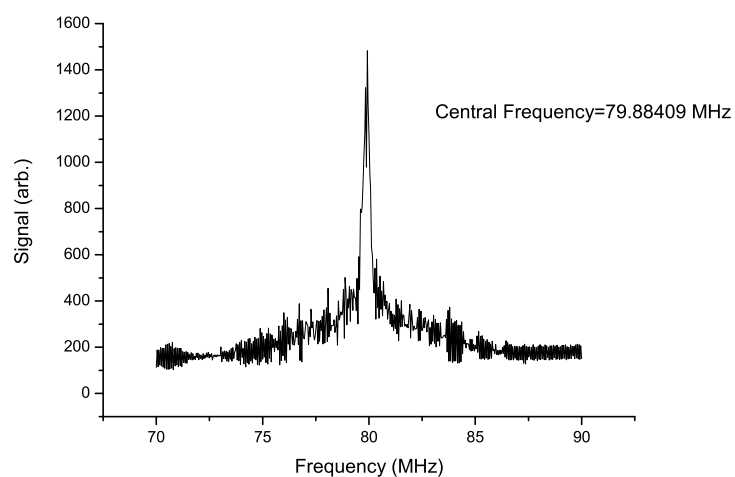


Figure 4.7: Frequency beat note of the master laser and the Ti:Sapphire laser at 1.2 W pumping.

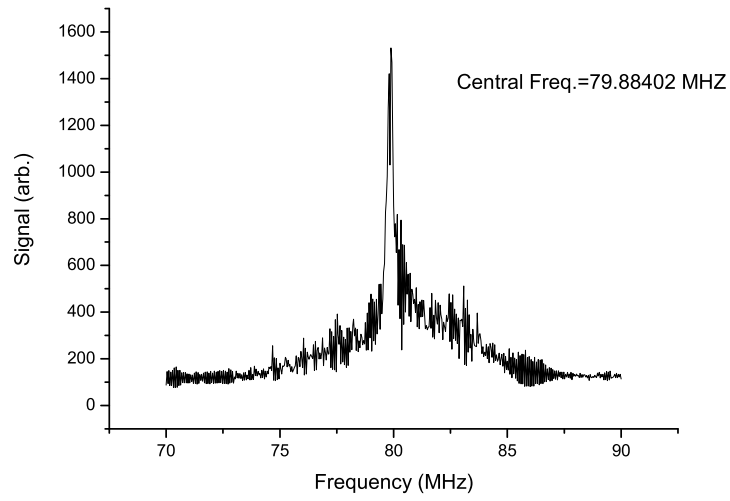


Figure 4.8: Frequency beat note of the master laser and the Ti:Sapphire laser at 1.4 W pumping.

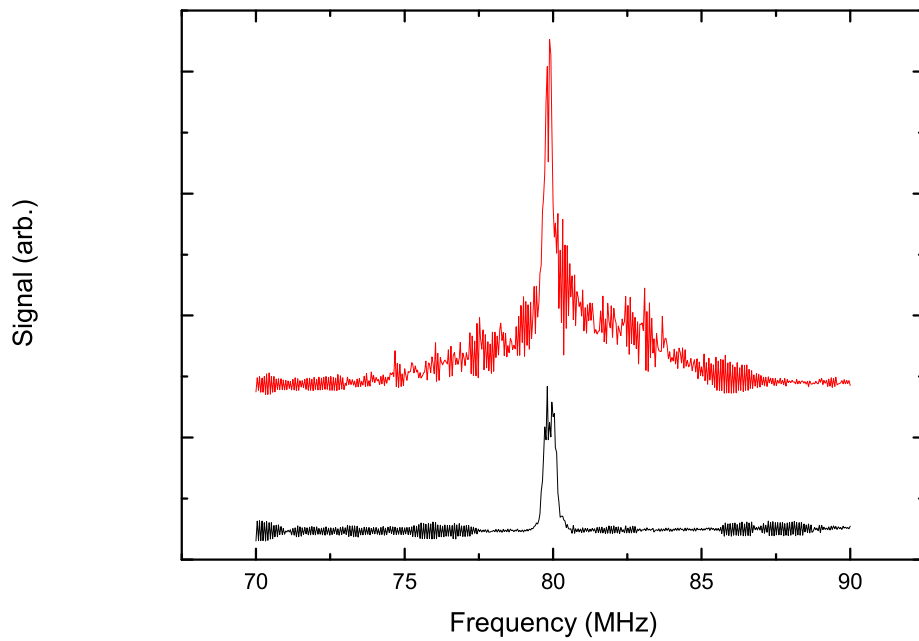


Figure 4.9: Optical frequency spectrum of the laser. The top curve shows the spectrum of the injection-locked Ti:Sapphire laser at 1.4 W pumping power. The bottom curve shows the spectrum of the master laser. The curves are offset vertically for clarity.

# Chapter 5

## Conclusion

We have demonstrated a cw injection-locked single-frequency Ti:Sapphire laser at 785 nm with the spectral linewidth less than 5 MHz and an output power of about 190 mW at 2 W pumping power. Injection-locked Ti:Sapphire laser eliminates the needs of birefringent filters and optical diodes in the conventional Ti:Sapphire laser and results much lower threshold power. The required pumping power is only 1.23 W. In comparison with self-lasing cw Ti:Sapphire, the cost of our system was largely reduced. The wavelength is determined by the wavelength of the diode laser used to inject the Ti:Sapphire laser. Stability of frequency is achieved by the injection-locking method, and may provide a good performance in laser spectroscopy.

### Future Work

1. Because the intensity noise is from vibration and acoustic noise, we can improve the intensity stability with a more rigid, stable Ti:Sapphire laser cavity.
2. Higher output power may be achieved as long as the signal-to-noise ratio of the error signal at higher pumping power can be optimize.

# References

- [1] S. HL and S. WH, Appl. Phys. Lett. **8**, 91 (1996).
- [2] N. Lesage, G. Mullet, Y. Andre, and G. Bourdet, Opt. Comm. **115**, 291 (1995).
- [3] P. Even, K. Ait-Ameur, and G. Stephan, Europhys. Lett. **36**, 179 (1996).
- [4] T. Fishman and A. Hardy, Appl. Opt. **39**, 3108 (2000).
- [5] C. N. Man and A. Brillet, Opt. Lett. **9**, 333 (1984).
- [6] T. Teyo, V. Sinivasagam, M. Abdullah, and H. Ahmad, Opt. Las. Technol **31**, 493 (1999).
- [7] B. Couillaud, A. Ducasse, E. Freysz, and L. Sarger, Opt. Lett. **9**, 435 (1984).
- [8] M. Margalit, M. Orenstein, and G. Eisenstein, Opt. Comm. **129**, 373 (1996).
- [9] J. Yu *et al.*, OC **132**, 263 (1996).
- [10] in *Lasers*, edited by A. Siegman (University Science Books, Mill Valley, 1986), p. 1129.
- [11] J.-C. Cotteverte, G. Ropars, A. L. Floch, and F. Bretenaker, IEEE J. Quantum Electron. **30**, 2516 (1994).
- [12] in *Fundamental of photonics*, edited by B. E. A. Saleh and M. C. Teich (Wiley. Interscience, ADDRESS, 1944), p. 712.
- [13] in *Quantum Electronics*, edited by A. Yariv (Wiley, ADDRESS, 1988).
- [14] J. M. Supplee, E. A. Whittaker, and W. Lenth, Appl. Opt. **33**, 6294 (1994).